Pure Appl. Chem., Vol. 83, No. 11, pp. 2041–2053, 2011.
doi:10.1351/PAC-CON-11-03-04

Polymer-embedded gold and gold/silver nanoparticle-modified electrodes and their applications in catalysis and sensors*

Shanmugam Manivannan and Ramasamy Ramaraj‡

Centre for Photoelectrochemistry, School of Chemistry, Madurai Kamaraj University, Madurai 625 021, India

Abstract: Metal nanoparticles encapsulated by silicate sol-gel matrix find numerous applications particularly in electrocatalysis and sensors. In our previous reports, we have reported the mono- and bi-metal gold, silver, and core/shell gold/silver nanoparticles embedded in functionalized silicate sol-gel matrices. Modified electrodes were fabricated using mono- and bi-metallic gold, silver, and core/shell gold/silver nanoparticles embedded in silicate sol-gel, and they were used for the electrocatalysis and sensing of H_2O_2 and simultaneous detection of hydrazine, sulfite, and nitrite. We have prepared the gold nanoparticles encapsulated by amine-functionalized silicate sol-gel matrix in a single step without using any external reducing agents. The gold nanoparticles were also synthesized by using amine-functionalized silane monomer in the presence of β-cyclodextrin (β-CD), resulting in metal/polymer core/shell nanostructures. This nanocomposite material showed a synergistic stabilizing effect when compared to either silicate sol-gel matrix or β-CD alone as stabilizer. The synthesized gold nanoparticles were characterized using UV–vis spectroscopy and high-resolution transmission electron microscopy. Modified electrodes were prepared by using the gold nanoparticles embedded in silicate sol-gel matrix, and their electrochemical characteristics were studied.

Keywords: β-cyclodextrins; electrocatalysis; gold nanoparticles; modified electrodes; silicate sol-gel matrix; sensors.

INTRODUCTION

Colloidal solutions of noble metals, especially those of gold (Au) nanoparticles and silver (Ag), have been studied extensively because of their intense absorption band in the visible region, often called surface plasmon resonance absorption. The modification of metal nanoparticles surface with different organic receptors has attracted wide attention because of their potential applications in catalysis, sensors and nonlinear optical materials and in the development of biological tracers as well as optoelectronic nanodevices [1–3]. Therefore, the synthesis of stable metal nanoparticles with different size and surface modification is a challenging task for researchers. It remains a challenge to develop facile and environmentally friendly methods for the synthesis of gold and silver nanoparticles with controlled size, shape and surface functionality. The Au/silica and Ag/silica nanoparticles find applications in sensing, and the thickness of the silica shell coat alters the optical property of the metal nanoparticles.

*Paper based on a presentation made at the International Conference on Nanomaterials and Nanotechnology (NANO-2010), Tiruchengode, India, 13–16 December 2010. Other presentations are published in this issue, pp. 1971–2113.

‡Corresponding author: E-mail: ramarajr@yahoo.com

The silica shell makes the gold and silver nanoparticles biocompatible [4,5] and these metal particles find applications in fluorescent bioimaging [6]. β-Cyclodextrin (β-CD) is a water-soluble and nontoxic cyclic oligosaccharide and has been extensively used in host-guest chemistry for constructing versatile supramolecular aggregates owing to their special hydrophobic cavities. Reducing and capping properties of the β-CD for preparing mono- and bi-metallic nanoparticles in alkaline solution have been explored [7,8]. Smaller metal nanoparticles were also prepared using β-CD as reducing agent when compared to other reducing agents [9].

Synthesis and stabilization of metal nanoparticles in silicate sol-gel matrix is a single-step procedure and yields uniform distribution of nanometer sized particles and shows versatility in the form of sols, gels, films, and monoliths. Lev et al. [10–13] and Wang et al. [14,15] have reported different modified electrodes using sol-gel chemistry. The H_2O_2 sensors are of practical importance in chemical, biological, clinical, environmental, and fuel cell applications [16–19]. The importance of selective and simultaneous sensing of toxic molecules has led to the designing of gold nanoparticles embedded in silicate sol-gel-based electrochemical sensors [20]. In the present article, we summarize some of our recent research work on the mono- and bi-metal gold, silver, and core/shell gold/silver nanoparticles embedded in functionalized silicate sol-gel matrix and their electrocatalytic applications [21–23]. We also report the synthesis (in situ approach) of β-CD-EDAS (*N*-[3-(trimethoxysilyl) propyl] ethylenediamine) matrix encapsulated gold nanoparticles (hereafter referred to as β-CD-Au-EDAS) and the preparation of corresponding chemically modified electrode. The GC/CD-Au-EDAS modified electrode showed a tuneable kinetic barrier when $[Fe(CN)_6]^{3-/4-}$ couple was used. The barrier property of the β-CD-EDAS composite material modified electrode (GC/EDAS or GC/CD-EDAS) was tailored to the desired level by introducing the gold nanoparticles (GC/CD-Au-EDAS). The gold nanoparticles provide the necessary conduction pathway besides acting as nanoscale electrode in promoting the electron transfer between the analyte and the electrode surface.

EXPERIMENTAL SECTION

MTMOS (methyltrimethoxysilane), APS [(3-aminopropyl)triethoxysilane], and EDAS monomers were purchased from Aldrich and were used for the preparation of corresponding silicate sol-gel. The β-CD-Au-EDAS was prepared by the following procedure (as shown in Fig. 1).

In a typical experiment, 25 μL of 1 M EDAS silane monomer was added to a 5 mL aqueous solution of 7 mM β-CD under vigorous stirring, and the stirring was continued for another 60 min to obtain homogeneous β-CD-EDAS matrix. To this solution 50 μL of 0.1 M $HAuCl_4$ was added under stirring. The color of the solution immediately turned dark yellow because of the ammine-chloride complex formation [10–13] between EDAS silane and $HAuCl_4$. The mixture was kept stirred for 48 h until the solution turned a wine red color, confirming the formation of β-CD-Au-EDAS. For the synthesis of Au-EDAS nanomaterial, the same procedure was used in the absence of β-CD. The preparation of gold and core/shell gold/silver nanoparticles embedded in methyl (MTMOS) or amine (APS) functionalized silicate sol-gel modified electrodes were already reported [21–23].

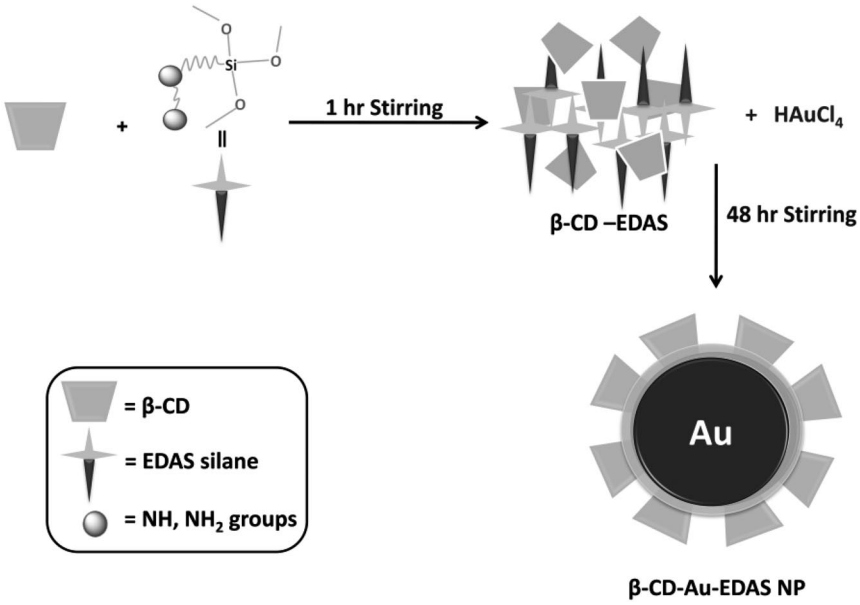

Fig. 1 Schematic preparation of the synthesis of β-CD-Au-EDAS nanomaterial.

The glassy carbon (GC) electrode (diameter = 3 mm, CH Instruments, USA) was twice polished using alumina powder (0.05 μm) followed by sonication in doubly distilled water for 3 min. The cleaned GC electrode was dried for 5 min at room temperature. A known volume of EDAS sol-gel or β-CD-EDAS composite or Au-EDAS nanomaterials or β-CD-Au-EDAS nanomaterials solution was casted on the bare GC electrode surface and allowed to dry at room temperature for 1 h (represented as GC/EDAS, GC/CD-EDAS, GC/Au-EDAS, and GC/CD-Au-EDAS). The dried electrode was then soaked in distilled water for 5 min and used for electrochemical experiments. The thickness of the film coated on the electrode was calculated as 1 μm [24].

The cyclic voltammograms of the modified electrodes were recorded using an EG&G Princeton Applied Research 283 Potentiostat/Galvanostat controlled by Echem software. Electrochemical experiments were performed using a single compartment three-electrode cell. The modified GC electrode was used as working electrode and platinum wire as counter electrode. The reference electrode was a saturated calomel electrode. The solution was deaerated by purging nitrogen gas for 25 min before each experiment.

RESULTS AND DISCUSSION

Gold nanoparticles embedded in MTMOS silicate sol-gel matrix modified electrode as an amperometric sensor for H_2O_2

The preformed gold nanoparticles were embedded in the MTMOS silicate sol-gel matrix by the ex situ approach, and its modified electrode was prepared (GC/MTMOS-Au) and characterized [21]. The electrochemical response observed for the GC/MTMOS-Au nanomaterials modified electrode revealed that the dispersed gold nanoparticles in the MTMOS film were in electrical contact with each other. The $[Fe(CN)_6]^{3-/4-}$ redox couple was used as a marker to probe the tunable kinetic barrier of the gold nanoparticles dispersed in the MTMOS silicate sol-gel matrix. The GC/MTMOS-Au modified electrode showed good electrocatalytic response for H_2O_2 reduction without an enzyme or mediator immobilized in the MTMOS silicate sol-gel. A linear relationship was observed for H_2O_2 sensing in the con-

centration range from 2.5 to 45 μM at the GC/MTMOS-Au modified electrode at an applied potential of –0.5 V, and the detection limit was calculated as 3.15 nM [21]. The GC/MTMOS-Au modified electrode was simple to prepare, and this electrode showed fast response, good stability, and reproducible results.

Core/shell gold/silver nanoparticles embedded in MTMOS silicate sol-gel matrix modified electrode as an electrocatalyst for the reduction of H_2O_2

The bimetallic nanoparticle-modified electrodes have been attracting attention in recent years since the addition of a second metallic component enhances the activity, selectivity, and stability of a pure monometal catalyst [25–27]. As the continuation of our previous work [21] of gold nanoparticles embedded in MTMOS silicate sol-gel matrix for the amperometric sensing of H_2O_2, the bimetallic core/shell gold/silver nanoparticles [$Au_{100-x}Ag_x$ (x = 15, 27, 46, and 60)] were embedded in MTMOS silicate sol-gel matrix by the ex situ approach and the modified electrode was used for the electrocatalytic reduction and amperometric sensing of H_2O_2 (Fig. 2) [22].

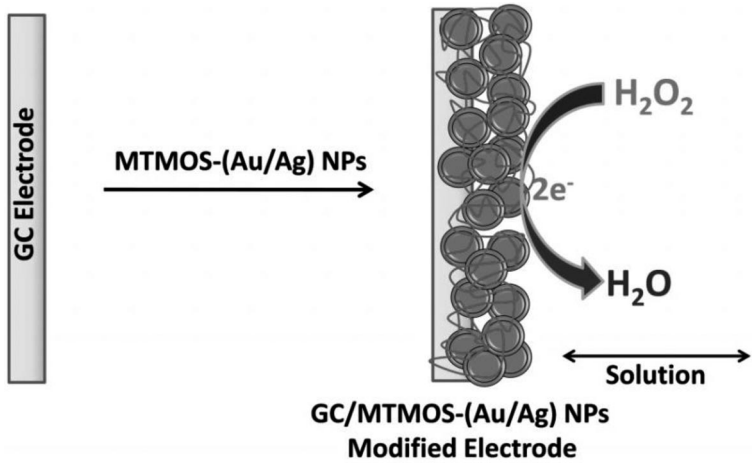

Fig. 2 Schematic representation of electrocatalytic reduction of H_2O_2 at the MTMOS-(gold/silver) bimetal core/shell nanoparticle-modified electrode.

The electrocatalytic activity of the core/shell $Au_{100-x}Ag_x$ (x = 15, 27, 46, and 60) bimetallic nanoparticles embedded in MTMOS silicate sol-gel matrix toward the reduction of H_2O_2 was investigated by using cyclic voltammetry and chronoamperometric techniques. The MTMOS silicate sol-gel matrix embedded $Au_{73}Ag_{27}$ core/shell nanoparticle-modified electrode showed better synergistic electrocatalytic effect toward the reduction of H_2O_2 when compared to monometal MTMOS-Au and MTMOS-Ag modified electrodes (Fig. 3). These modified electrodes were studied without immobilizing any enzyme in the MTMOS silicate sol-gel matrix. This study highlights the influence of the molar composition of silver nanoparticles in the gold/silver bimetallic composition on the electrocatalytic reduction and sensing of H_2O_2 in comparison to monometal gold and silver nanoparticles.

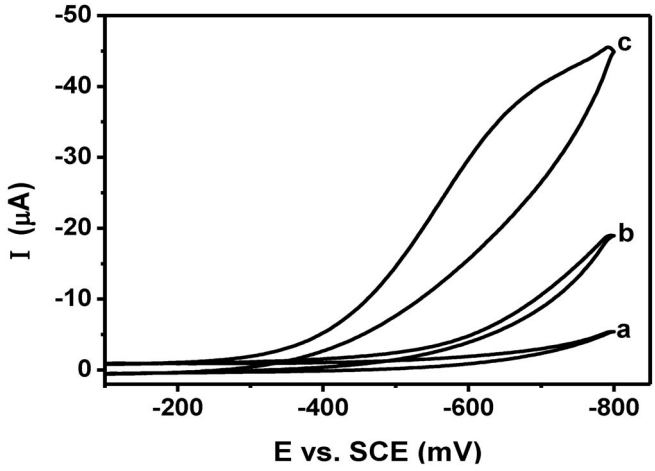

Fig. 3 Cyclic voltammograms recorded for 1 mM of H_2O_2 at GC/MTMOS-Ag (a), GC/MTMOS-Au (b), and GC/MTMOS-$Au_{73}Ag_{27}$ (c) modified electrodes in 0.1 M PBS (pH = 7.2) at a scan rate of 50 mV s^{-1}. (Reprinted with kind permission of Springer Science + Business Media [22].)

Simultaneous electrochemical sensing of toxic molecules at the gold nanoparticles embedded in APS silicate sol-gel matrix

The gold nanoparticles encapsulated by APS silicate sol-gel matrix were synthesized using $NaBH_4$ as an external reducing agent by the in situ method and its modified electrode was prepared (GC/APS-Au) [23]. The GC/APS-Au modified electrode was used for the electrocatalysis and electrochemical sensor application toward the simultaneous detection of N_2H_4, SO_3^{2-}, and NO_2^-. The GC/APS-Au electrode efficiently electrocatalyzed the oxidation of N_2H_4, SO_3^{2-}, and NO_2^- at 0.05, 0.2, and 0.55 V, respectively (Fig. 4A), and a large decrease in the overpotential to an extent of ~750, ~600, and ~250 mV, respectively was observed [23].

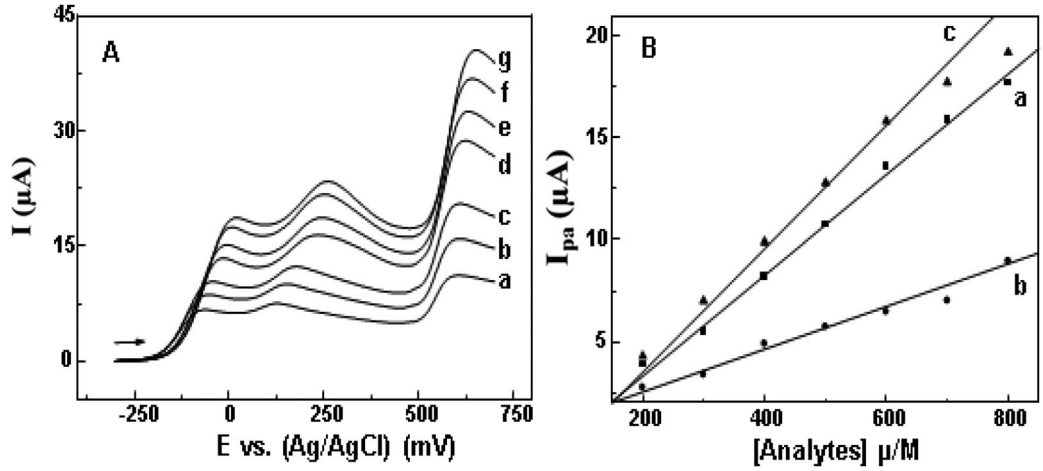

Fig. 4 (A) Linear sweep voltammograms obtained for the mixture of N_2H_4, SO_3^{2-}, and NO_2^- with successive addition of their concentrations in 200 μM (a), 300 μM (c), 400 μM (d), 500 μM (e), 600 μM (f), 700 μM (g), and 800 μM (h) in 0.1 M PBS (pH 7.2) at GC/APS-Au electrode. (B). Corresponding calibration plots. (Reprinted with kind permission of Elsevier [23].)

The linear sweep voltammetric responses obtained for the mixture of N_2H_4, SO_3^{2-}, and NO_2^- at the GC/APS-Au electrode with successive additions of their concentrations showed a linear calibration plot for the anodic peak currents of analytes with increase in concentrations of analytes and the sensitivity of this system was found to be 0.0241 ± 0.0007, 0.0098 ± 0.0007, and 0.2577 ± 0.0012 μA/μM toward the electrooxidation of N_2H_4, SO_3^{2-}, and NO_2^-, respectively (Fig. 4B).

Preparation and characterization of β-CD-Au-EDAS nanoparticles

The in situ surface modification of the nanomaterials by introducing different reagents and synthetic approaches is one of the current trends in contemporary research. The optical properties of the gold nanoparticles are strongly dependent on size and surface modification and can be easily monitored through UV–vis absorption spectroscopy by following the surface plasmon resonance band [28–33]. In the present work, sub-10 nm-sized gold nanoparticles were synthesized using β-CD-EDAS composite without using any external reducing agent.

The absorption spectra of the mixture of $HAuCl_4$ and β-CD were recorded after 48 h of stirring. The $HAuCl_4$ showed a band at 313 nm, and the mixture of $HAuCl_4$ and β-CD showed a new low intensity band at 575 nm in addition to the 313 nm band due to the poor formation of gold nanoparticles (Fig. 5a). The addition of EDAS to $HAuCl_4$ led to the formation of a small amount of Au-EDAS (band at 571 nm) (Fig. 5b) after 48 h of stirring. When β-CD and EDAS were mixed with $HAuCl_4$ and stirred for 48 h, the clear formation of β-CD-Au-EDAS was observed (Fig. 5c). The formation of β-CD-Au-EDAS was complete in 48 h of stirring, and the surface plasmon resonance band was observed at 535 nm, revealing the formation of β-CD-Au-EDAS. Among the three different synthetic approaches, it was observed that the efficient reduction and stabilization took place in the presence of a mixture of β-CD and EDAS silicate sol-gel composite.

The aqueous solution of β-CD showed a pH of 4.86 and the mixture of EDAS and β-CD showed a pH of 9.44. The deprotonated β-CD (1° hydroxyl groups) at pH 9.44 acts as a nucleophile and reduces the $AuCl_4^-$ to gold nanoparticles. During the reduction of the metal precursor the 1° hydroxyl groups of the β-CD are oxidized into –COOH groups which play the role of stabilizer and at the same time 2° hydroxyl groups of β-CD are not oxidized [34,35]. In addition, the –NH– and $–NH_2$ groups present in the EDAS silicate sol-gel matrix are also partially involved in the reduction of $AuCl_4^-$ into gold nanoparticles [10–13]. The efficient reduction of $AuCl_4^-$ was not observed by β-CD alone under depro-

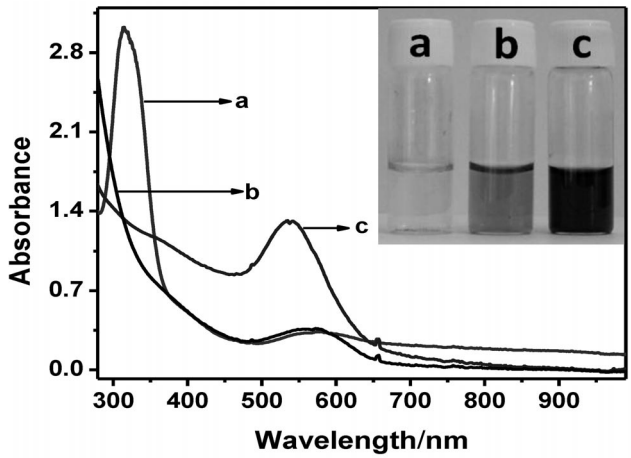

Fig. 5. Absorption spectra recorded for $HAuCl_4$-CD mixture (a), Au-EDAS (b), and β-CD-Au-EDAS (c). Reaction mixtures were vigorously stirred for 48 h.

tonated condition. The absorption peak observed at 312 nm (Fig. 5a) was attributed to the $HAuCl_4$ in the presence of β-CD molecules. The diffused reflectance spectra were recorded for the EDAS silicate sol-gel matrix (Fig. S1a), β-CD-EDAS composite (Fig. S1b), Au-EDAS (Fig. S1c), and β-CD-Au-EDAS (Fig. S1d) films. The diffused reflectance spectra of EDAS silicate sol-gel and CD-EDAS did not show any band in the visible region (Fig. S1a,b). The Au-EDAS film showed the surface plasmon resonance band at 547 nm due to the gold nanoparticles. The β-CD-Au-EDAS film showed the surface plasmon resonance band at 581 nm. A shift in the surface plasmon resonance band for the gold nanoparticles was noticed for the film samples due to the stabilization of gold nanoparticles by EDAS silicate sol-gel and CD-EDAS composite in the solid state.

The high-resolution transmission electron microscopy (HRTEM) and energy dispersive X-ray analysis (EDX) were recorded for the β-CD-Au-EDAS, and the images are shown in Fig. 6 and Fig. S2. The so-formed spherical core/shell Au/EDAS silicate sol-gel nanostructures (β-CD-Au-EDAS) were confirmed from the HRTEM images. The core/shell structure was distinguished from the contrast difference in the images between the two components. In a single nanoparticle, the dark spot was correlated to the gold nanoparticle and the diffused image was correlated to the EDAS silicate sol-gel matrix encapsulated gold nanoparticle core (Fig. S2B). Figure 6B shows the selected-area electron diffraction

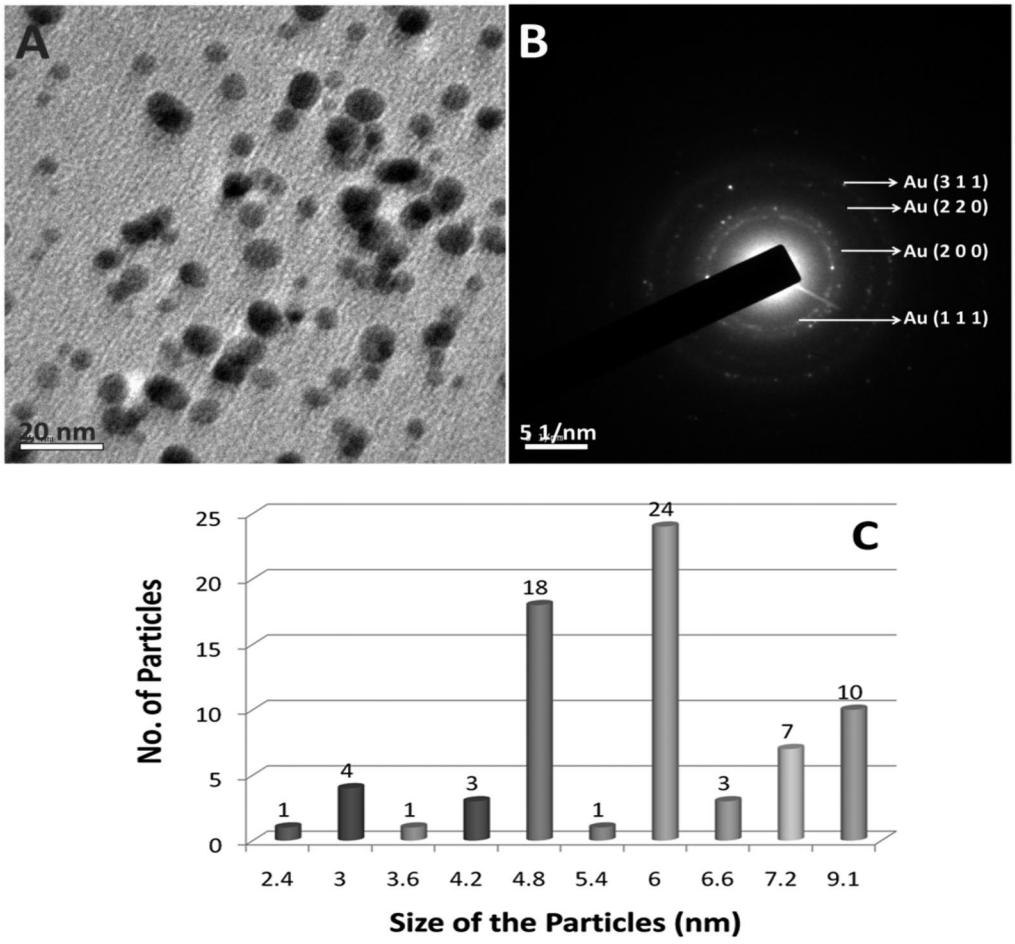

Fig. 6 HRTEM image of core/shell β-CD-Au-EDAS nanostructures (A) and the SAED pattern (B). Histogram of β-CD-Au-EDAS (C). Fig. 6A was considered for particle size analysis.

(SAED) pattern of the β-CD-Au-EDAS and the calculated crystal plane values of gold ((1 1 1), (2 0 0), (2 2 0), and (3 1 1)) (Fig. 6B) are in agreement with the data base values of gold nanoparticles. Figure 6C represents the histogram of β-CD-Au-EDAS calculated from Fig. 6A. Due to the EDAS silicate sol-gel matrix encapsulation, the size of the gold nanoparticles was observed in the range from 2.4 to 9 nm with an average particle size of 6 nm.

Electrochemical behavior of β-CD-Au-EDAS nanoparticle-modified electrodes

In order to understand the electrochemical properties of the β-CD-Au-EDAS modified electrode, the cyclic voltammograms were recorded for the GC/CD-Au-EDAS modified electrode in 0.5 M H_2SO_4 and 0.2 M PBS (pH 6.8). The characteristic oxidation peak [20] due to the gold nanoparticles was observed at 0.9 V as a low intense peak (Fig. S3). The electrochemical behavior of the $[Fe(CN)_6]^{3-/4-}$ redox couple at the GC/CD-Au-EDAS modified electrode was studied to understand the kinetic barrier of the modified electrode. At this β-CD-Au-EDAS modified electrode the $[Fe(CN)_6]^{3-/4-}$ couple exhibits reversible behavior (Fig. 8A). However, two pairs of redox waves were observed for the $[Fe(CN)_6]^{3-/4-}$ couple at the GC/CD-Au-EDAS modified electrode, one due to the irreversibly adsorbed $[Fe(CN)_6]^{3-/4-}$ species and the other due to the freely diffused $[Fe(CN)_6]^{3-/4-}$ species through the pinholes of the swelled GC/CD-Au-EDAS electrode. Similar results were also observed at the GC/EDAS, GC/CD-EDAS, and GC/Au-EDAS modified electrodes (Fig. 8A). The electron transfer between the redox species in solution and the electrode must occur by electron hoping through the fixed redox molecules and/or by diffusion through the defects (pinholes present in the porous EDAS matrix), and hence it is predicted that the redox couple gets irreversibly adsorbed or freely diffusing through the pores of the EDAS silicate sol-gel film. The electron transfer that occurs between the electrode surface and the $[Fe(CN)_6]^{3-/4-}$ species gives rise to the two characteristic redox peaks due to the irreversibly adsorbed redox species and freely diffused species through the pinholes. The schematic representation of the modified electrode and the irreversibly adsorbed $[Fe(CN)_6]^{3-/4-}$ couple in the CD-Au-EDAS film are shown in Fig. 7.

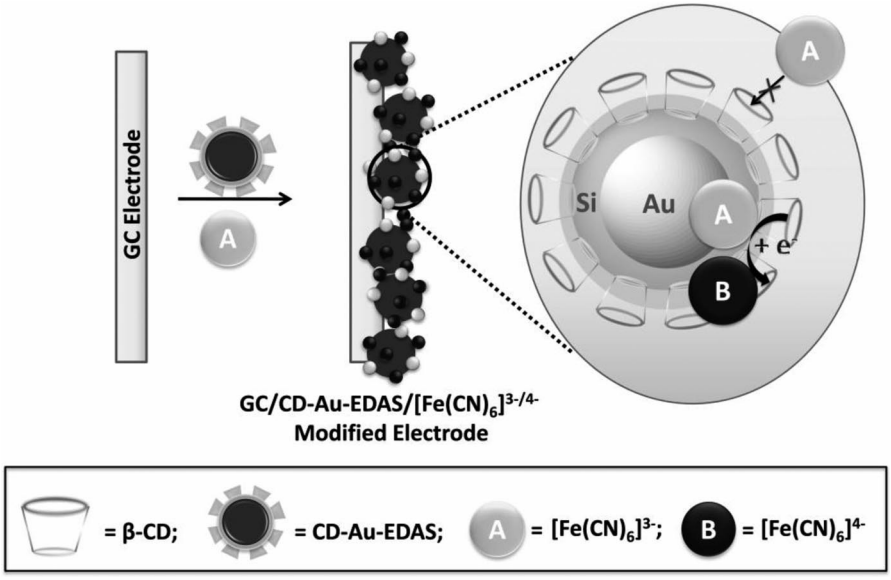

Fig. 7 Schematic representation of the GC/CD-Au-EDAS modified electrode and the adsorption of $[Fe(CN)_6]^{3-/4-}$ species.

The electrochemistry of $[Fe(CN)_6]^{3-/4-}$ couple adsorbed or precipitated at the electrode surface is of great interest both for analytical and electrode mechanism studies. Oyama and co-workers [36–38] and Murray co-workers [39] have made significant contributions in the field of modified electrodes with multiply charged metal complexes electrostatically bound to the polyelectrolyte film and the electrode kinetics of the surface confined metal complexes at the polymer coatings were studied. The electrochemical behavior of the $[Fe(CN)_6]^{3-/4-}$ species confined to the other modified electrodes has already been studied [40–43].

The typical cyclic voltammograms observed for $[Fe(CN)_6]^{3-/4-}$ species at diffusion mode (A) and adsorption mode (B) are shown in Fig. 8. The peak currents at the modified electrodes were 2–5 times

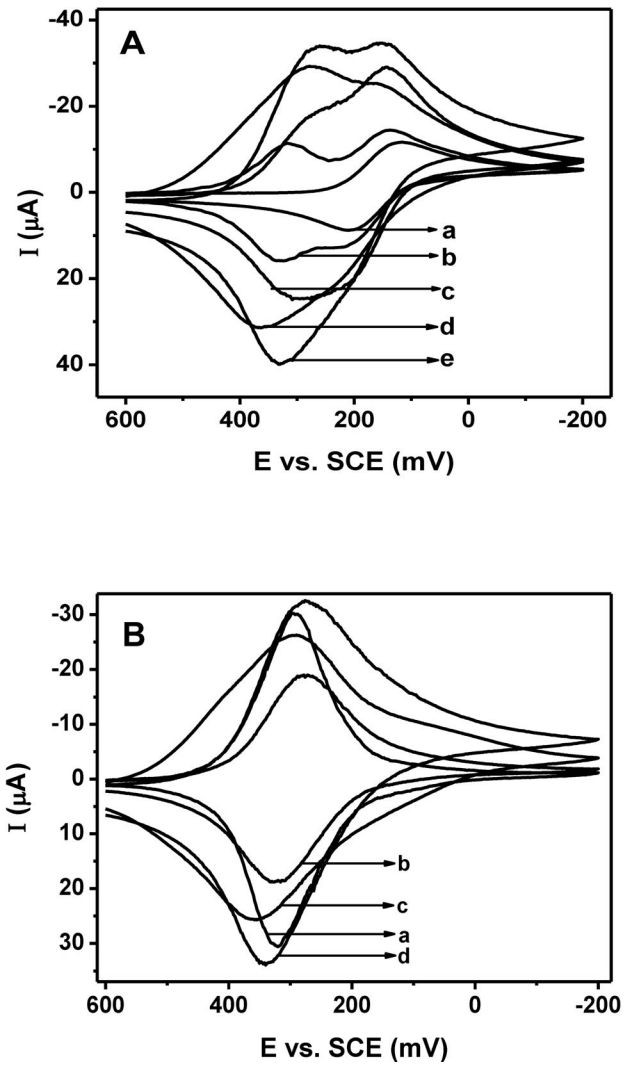

Fig. 8 (A): Cyclic voltammograms observed for $[Fe(CN)_6]^{3-}$ present in solution at bare GC (a), GC/EDAS (b), GC/CD-EDAS (c), GC/Au-EDAS (d), and GC/CD-Au-EDAS (e) in 0.1 M KCl at a scan rate of 50 mV s^{-1}. (B): Cyclic voltammograms of $[Fe(CN)_6]^{3-}$ incorporated at the modified electrodes: GC/EDAS (a), GC/CD-EDAS (b), GC/Au-EDAS (c), and GC/CD-Au-EDAS (d). The electrodes were dipped in 1 mM $K_3Fe(CN)_6$ solution for 10 min prior to the experiment and washed and dipped in 0.1 M KCl supporting electrolyte.

higher than that of the bare GC electrode due to the preconcentration of the $[Fe(CN)_6]^{3-/4-}$ species at the modified electrode (Figs. 8A,B). The $[Fe(CN)_6]^{3-/4-}$ species were irreversibly adsorbed into the EDAS silicate sol-gel film. At the GC/EDAS modified electrode the $[Fe(CN)_6]^{3-/4-}$ couple exhibited two peaks at 177 and 320 mV ($E_{1/2}$) for diffused and adsorbed species (Fig. 8A-b), respectively with a difference of 142 mV between the two redox potential. The observed positive shift in the redox potential for the surface-confined redox species at the solvent swollen film suggests that this system can effectively be utilized as an immobilized electrocatalyst for electrocatalytic reduction/oxidation reactions. The presence of β-CD molecules at the GC/CD-EDAS and GC/CD-Au-EDAS modified electrodes increased the peak currents (Figs. 8A-c–e) when compared to the GC/Au-EDAS modified electrode. The apparent redox potential differences between the irreversibly adsorbed redox species and the freely diffused species are as follows: 118, 136, and 137 mV for the GC/CD-EDAS, GC/Au-EDAS and GC/CD-Au-EDAS modified electrodes, respectively.

The electrochemical responses observed for the $[Fe(CN)_6]^{3-}$ incorporated GC/EDAS, GC/CD-EDAS, GC/Au-EDAS, and GC/CD-Au-EDAS modified electrodes dipped in 0.1 M KCl are shown in Fig. 8B. The anodic to cathodic peak potential difference (ΔE_p) of ~20 mV was observed for the $[Fe(CN)_6]^{3-/4-}$ couple at the GC/EDAS modified electrode, suggesting the surface-confined redox molecule behavior. The GC/CD-EDAS, GC/Au-EDAS, and GC/CD-Au-EDAS at the modified electrodes showed ΔE_p values of 47, 59, and 64 mV, respectively. Further, the shape of the cyclic voltammograms and their peak separation were found to vary with the adsorbed $[Fe(CN)_6]^{3-/4-}$ species concentration in the coated film (Γ). When Γ is relatively low (0.8221×10^{-9} M) at the GC/EDAS modified electrode, the shape of the cyclic voltammogram is similar to that expected for a surface-confined species, i.e., the peaks are nearly symmetrical and anodic to cathodic peak separation, ΔE_p, is ~20 mV. The calculated Γ values increased in the order of GC/CD-EDAS (9.3382×10^{-9} M) < GC/Au-EDAS (1.9129×10^{-8} M) < GC/CD-Au-EDAS (1.9766×10^{-8} M) modified electrodes and the electrochemical behavior was more like diffusion controlled with broad peaks with a diffusional tail and higher ΔE_p values. It is inferred that the incorporation of gold nanoparticles at the GC/EDAS and GC/CD-EDAS modified electrodes led to an increase in the peak-to-peak separation from 20 to 59 mV for GC/Au-EDAS and from 48 to 64 mV for GC/CD-Au-EDAS modified electrodes (Fig. 8B). These ΔE_p values of 59 and 64 mV are significantly close to the Nernstian value of 62 mV found for the $[Fe(CN)_6]^{3-/4-}$ species present in solution [40–43]. Further, the $[Fe(CN)_6]^{3-/4-}$ species are sterically incapable of complexing with β-CD, since the size of $[Fe(CN)_6]^{3-/4-}$ species is larger than the β-CD cavity size [44,45]. The gold nanoparticles provide the necessary conduction pathway besides acting as nanoscale electrode in promoting the electron transfer between the analyte and the electrode surface at the GC/Au-EDAS and GC/CD-Au-EDAS modified electrodes (Figs. 8B-c,d). The increase in the peak current at the GC/CD-Au-EDAS modified electrode was higher than that at the GC/Au-EDAS modified electrode even though an equal amount of gold nanoparticles was maintained at both the modified electrodes (Figs. 8-Bc,d). It can be explained based on the size-dependent electrochemical properties of the gold nanoparticles [46,47] that the so-formed size of the gold nanoparticles in the presence of β-CD (CD-Au-EDAS) is much smaller than that of the Au-EDAS system. It is acceptable that the smaller gold nanoparticles at the β-CD-Au-EDAS modified electrode with higher active surface area are expected to show a better electron-transfer process than those of Au-EDAS modified electrode. Figure 9 shows the continuous cyclic voltammogram (25 cycles) recorded for GC/CD-Au-EDAS/$[Fe(CN)_6]^{3-}$ modified electrode and the stable cyclic voltammograms reveal the durability and stability of the irreversibly adsorbed $[Fe(CN)_6]^{3-/4-}$ species at the GC/CD-Au-EDAS modified electrode when dipped in 0.1 M KCl. Further work on the applications of these modified electrodes is under progress.

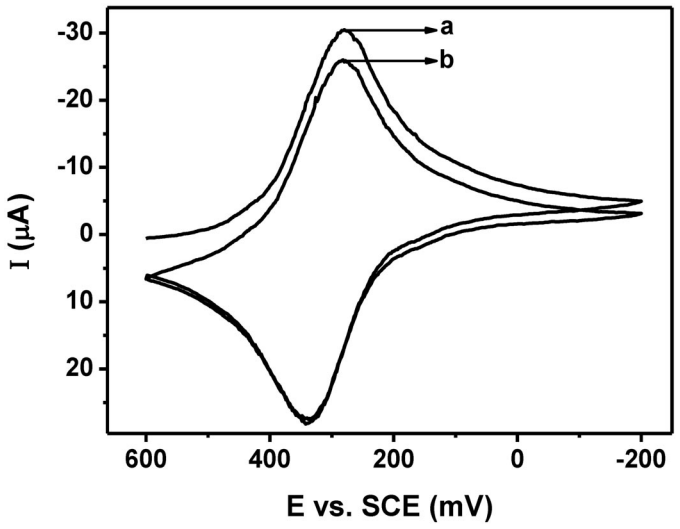

Fig. 9 Continuous cyclic voltammograms recorded for GC/CD-Au-EDAS/$[Fe(CN)_6]^{3-}$ modified electrode ($[Fe(CN)_6]^{3-/4-}$ irreversibly adsorbed at the modified electrode). GC/CD-Au-EDAS modified electrode soaked in 1 mM $K_3Fe(CN)_6$ solution for 10 min and washed. Number of continuous cycles: 1 (a) and 25 (b) cycles at a scan rate of 50 mV s^{-1}.

SUMMARY

The gold and gold/silver core/shell nanoparticles embedded in silicate sol-gel modified electrodes were prepared and used as an amperometric sensor for the detection of H_2O_2 and simultaneous detection of N_2H_4, SO_3^{2-}, and NO_2^-. The gold nanoparticles encapsulated in EDAS silicate sol-gel matrix in the presence of β-CD (core/shell Au/EDAS) were synthesized in a single step without using any external reducing agent. Modified electrodes were prepared using this core/shell Au/EDAS nanocomposite material (CD-Au-EDAS), and the electrochemical behavior of irreversibly adsorbed $[Fe(CN)_6]^{3-}$ species at the GC/CD-Au-EDAS modified electrode was studied. The gold nanoparticles provide the necessary electron conduction pathway besides acting as nanoscale electrodes in promoting the electron transfer between the analyte and the electrode surface. The $[Fe(CN)_6]^{3-/4-}$ species were confined at the swelled CD-Au-EDAS film coated on the GC electrode.

SUPPLEMENTARY INFORMATION

Figures S1–S3 are available online (doi:10.1351/PAC-CON-11-03-04).

ACKNOWLEDGMENTS

RR acknowledges the financial support from the Department of Science and Technology (DST), New Delhi. SMV is a recipient of a CSIR-SRF fellowship. The HRTEM images were recorded at the Indian Institute of Technology (IIT), Chennai.

REFERENCES

1. P. M. Tessier, O. D. Velev, A. T. Kalambur, J. F. Rabolt, A. M. Lenhoff, E. W. Kaler. *J. Am. Chem. Soc.* **122**, 9554 (2000).
2. T. K. Sau, A. Pal, T. Pal. *J. Phys. Chem. B* **105**, 9266 (2001).
3. C. P. Collier, R. J. Saykally, J. J. Shiang, S. E. Henrichs, J. R. Heath. *Science* **277**, 1978 (1997).
4. A. Kumar, V. L. Pushparaj, S. Murugesan. *Langmuir* **22**, 8631 (2006).
5. P. Botella, A. Corma, M. T. Navarro. *Chem. Mater.* **19**, 1979 (2007).
6. S. Nagarajan, Z. Yong. *Recent Pat. Biomed. Eng.* **1**, 34 (2008).
7. P. Surojit, K. G. Sujit, P. Snigdhamayee, P. Sudipa, B. Soumen, J. Subhra, P. Anjali, T. Tatsuya, P. Tarasankar. *J. Phys. Chem. C* **111**, 10806 (2007).
8. H. B. N. Choon, Y. Jiexiang, Y. F. Wai. *J. Phys. Chem. C* **112**, 4141 (2008).
9. L. Yali, B. M. Keith, B. Pierre, H. T. L. Jhon. *Chem. Mater*. **15**, 4172 (2003).
10. O. Lev, M. Tsionsky, L. Rabinovich, V. Glezer, S. Sampath, I. Pankratov, J. Gun. *Anal. Chem*. **67**, 22A (1995).
11. O. Lev, Z. Wu, S. Bharathi, A. Modestov, V. Glezer, J. Gun, L. Rabinovich, S. Sampath. *Chem. Mater*. **9**, 2354 (1997).
12. M. Tsionsky, O. Lev. *Anal. Chem*. **67**, 2409 (1995).
13. K. Ramanathan, D. Avnir, A. Modestov, O. Lev. *Chem. Mater*. **9**, 2533 (1997).
14. J. Wang, P. V. A. Pamidi, D. S. Park. *Anal. Chem*. **68**, 2705 (1996).
15. J. Wang, P. V. A. Pamidi, D. S. Park. *Electroanalysis* **9**, 52 (1997).
16. S. D. Holmstrom, J. A. Cox. *Anal. Chem*. **72**, 3191 (2000).
17. M. D. Rubianes, G. A. Rivas. *Electrochem. Commun*. **5**, 689 (2003).
18. M. D. Rubianes, G. A. Rivas. *Electroanalysis* **17**, 73 (2005).
19. T. Tetsu, W. Tadashi. *Anal. Chem.* **63**, 1580 (1991).
20. S. Garrod, M. E. Bollard, A. W. Nicholls, S. C. Connor, J. Connelly, J. K. Nicholson, E. Holmes. *Chem. Res. Toxicol*. **18**, 115 (2005).
21. G. Maduraiveeran, R. Ramaraj. *J. Electroanal. Chem*. **52**, 58 (2007).
22. S. Manivannan, R. Ramaraj. *J. Chem. Sci.* **121**, 735 (2009).
23. G. Maduraiveeran, R. Ramaraj. *Electrochem. Commun.* **9**, 2051 (2007).
24. K. Sbkhoo. *Anal. Chem.* **74**, 5734 (2002).
25. S. Michael, A. Nashner, I. Frenkel, L. A. David, R. S. John, G. N. Ralph. *J. Am. Chem. Soc.* **119**, 7760 (1997).
26. L. Lehui, W. Haishui, Z. Yonghui, X. Shiquan, Z. Hongjie, H. Jiawen, Z. Bing. *Chem. Commun.* **2**, 144 (2002).
27. R. Alain, S. Jurgen, P. Henri. *Chem. Rev*. **102**, 3757 (2002).
28. J. Zheng, P. R. Nicovich, R. M. Dickson. *Annu. Rev. Phys. Chem*. **58**, 409 (2007).
29. C. M. Aikens, S. Z. Li, G. C. Schatz. *J. Phys. Chem. C* **112**, 11272 (2008).
30. K. L. Kelly, E. Coronado, L. L. Zhao, G. C. Schatz. *J. Phys. Chem. B* **107**, 668 (2003).
31. M. Hu, J. Y. Chen, Z. Y. Li, L. Au, G. V. Hartland, X. D. Li, M. Marquez, Y. N. Xia. *Chem. Soc. Rev.* **35**, 1084 (2006).
32. A. Moores, F. Goettmann. *New J. Chem.* **30**, 1121 (2006).
33. H. Wang, D. W. Brandl, P. Nordlander, N. Halas. *Acc. Chem. Res*. **40**, 53 (2007).
34. C. Fraschini, M. R. Vignon. *Carbohydr. Res.* **328**, 585 (2000).
35. M. E. Deary, D. M. Davies. *Carbohydr. Res.* **309**, 17 (1998).
36. N. Oyama, F. C. Anson. *Anal. Chem.* **52**, 1192 (1980).
37. N. Oyama, T. Ohsaka, T. Ushirogouchi. *J. Phys. Chem.* **88**, 5274 (1984).
38. N. Oyama, T. Ohsaka, H. Yamamoto, M. Kanekot. *J. Phys. Chem.* **90**, 3850 (1986).
39. R. W. Murray. *Acc. Chem. Res.* **13**, 135 (1980).
40. N. Oyama, F. C. Anson. *J. Electrochem. Soc.* **127***,* 640 (1980).

41. N. Oyama, S. Yamaguchi, Y. Nishiki, K. Tokuda, H. Matsuda, F. C. Anson. *J. Electroanal. Chem.* **139**, 371 (1982).
42. J. Facci, R. W. Murray. *J. Electroanal. Chem.* **124**, 339 (1981).
43. N. Oyama, T. Ohsaka, M. Kaneko, K. Sato, H. Matsudai. *J. Am. Chem. Soc*. **105**, 6003 (1983).
44. P. He, J. Ye, Y. Fang, I. Suzuki, T. Osa. *Electroanalysis* **9**, 68 (1997).
45. Y. Macda, T. Fukuda, H. Yamomoto, H. Kitano. *Langmuir* **13**, 4187 (1997).
46. B. K. Jena, C. R. Raj. *J. Phys. Chem. C* **111**, 15146 (2007).
47. P. Kalimuthu, S. A. John. *J. Electroanal. Chem.* **617**, 164 (2008).

